Sliding wear behaviour of alumina/nickel nanocomposites processed by a conventional sintering route

T. Rodriguez-Suarez [a,*], J.F. Bartolomé [b], A. Smirnov [b,c], S. Lopez-Esteban [a], R. Torrecillas [a], J.S. Moya [b]

[a] *Centro de Investigación en Nanomateriales y Nanotecnología (CINN), Consejo Superior de Investigaciones Científicas (CSIC), Universidad de Oviedo (UO), Principado de Asturias (PA), EDIFICIO FUNDACIÓN ITMA, Parque Tecnológico de Asturias, 33428 Llanera (Asturias), Spain*
[b] *Instituto de Ciencia de Materiales de Madrid (ICMM), Consejo Superior de Investigaciones Científicas (CSIC). C/Sor Juana Inés de la Cruz, 3, 28049 Cantoblanco (Madrid), Spain*
[c] *Department of Materials Engineering, Tallinn University of Technology, Ehitajate tee 5, 19086 Tallinn, Estonia*

Abstract

The wear resistance of Al_2O_3/2.5 vol.% Ni nanocomposites sintered by a conventional route was studied under ball-on-disk dry sliding conditions and compared with the same nanocomposites but consolidated by spark plasma sintering, together with alumina obtained by the same technique and by hot pressing. The results showed an improvement of about 0.5, 1 and 2 orders of magnitude, respectively. Thus, alumina/Ni nanocomposites processed by conventional route can compete, in cost and wear performance, with nanomaterials obtained by more sophisticated techniques.
© 2011 Elsevier Ltd. All rights reserved.

Keywords: Sintering; Nanocomposites; Mechanical properties; Wear resistance; Al_2O_3; Wear parts

1. Introduction

Ceramic/metal nanocomposites are of great interest due to the singularity they present: by the inclusion of secondary metallic phases in an appropriate content (below the percolation and aggregation threshold), particle grain size is limited to the nanoscale (20–60 nm) and matrix hardness can be improved up to ≈30%.[1,2–4] The particular case of ceramic/*n*Ni system has been widely studied.[2,3,5–8] These nanocomposites could find applications such as bearings and different purpose cutting tools.[9] In this sense, the study of friction and wear of ceramic/metal nanocomposites has received increasing attention from the scientific, technical and practical points of view.

In a previous work, alumina/Ni nanocomposites obtained by spark plasma sintering (SPS), gave maximum hardness values of 25 GPa for a 2.5 vol.% Ni content, and showed an excellent wear behaviour never reported before in the literature.[3] It was stated that the wear regime reached under diamond grinding wear test performed[10] (distilled water lubricated) was abrasion, where no pull-out was observed, and hardness was the mechanical property controlling the wear behaviour.

Nowadays, the spark plasma sintering technique has been widely extended on materials consolidation. This technique has many advantages, but presents some negative aspects such as the carbon diffusion from the graphite die and the reactive sintering that forms undesired phases in monolithic materials or composites,[4] as well as the effects of electrical current pulses (heating source) and residual stresses induced to materials by the high heating and cooling rates.

SPSed materials, present the advantage of retaining the nanostructure, hence, mechanical properties can be improved according to the smaller grain and flaw sizes. On the other hand, by conventional sintering (CS), certain grain growth is, in some way, expected.

In any case, CSed composites present the main advantage of being much easier to scale up. The present work is just focused to compare the friction and dry sliding wear behaviour of alumina/*n*Ni obtained by both SPS and a simple and conventional low cost processing route.

* Corresponding author. Tel.: +34 985 98 00 58; fax: +34 985 26 55 74.
E-mail address: t.rodriguez@cinn.es (T. Rodriguez-Suarez).

2. Experimental procedure

2.1. Powder synthesis

As starting materials, α-alumina powder (99.99%, Taimei Chemical Co., Ltd., Japan with $d_{50} = 0.20\,\mu m$ and a BET specific surface area of $14.5\,m^2/g$) and Nickel (II) nitrate hexahydrate (Merck, Germany, 99.0% purity, $(Ni(NO_3)_2 \cdot 6H_2O)$) were used.

Nickel precursor was weighed in order to have 2.5 vol.% metal content in the final composites and was initially dissolved in anhydrous ethanol by ultrasonic agitation. Subsequently, alumina powder was mixed with this alcoholic solution and ball milled for 24 h with Al_2O_3 balls. The mixture was dried at 120 °C, ground in an agate mortar and then, calcined at 400 °C for 2 h in air to obtain Al_2O_3/NiO mixed powders which were sieved down to 32 μm and, finally, reduced in a 90%Ar/10%H_2 atmosphere at 500 °C for 2 h yielding Al_2O_3/nNi powder.

2.2. Sintering

Two different approaches for nanocomposites sintering were studied: (i) the conventional sintering employing a horizontal tubular furnace (Forns Hobersal, ST. model, Spain) under a 90%Ar/10%H_2 atmosphere, and (ii) spark plasma sintering (FCT Systeme GMBH, HPD25, Germany) under vacuum conditions.

2.2.1. Conventional sintering (CS)

Al_2O_3/Ni powders were isostatically pressed at 200 MPa; the resulting pieces were fired using a tubular furnace under a 90%Ar/10%H_2 atmosphere in two steps: (i) at 500 °C for 2 h in order to reduce the possible nickel passivation and (ii) at 1400 °C for 2 h for final sintering. Heating and cooling rates were maintained at 10 °C/min.

2.2.2. Spark plasma sintering (SPS)

Cylindrical samples with a diameter of 20 and 40 mm and height of 2–4 mm were prepared as follows; (i) the sample were heated from room temperature to 600 °C at a rate of 600 °C/min, using a pressure of ~10 MPa; (ii) From 600 °C to 1100 °C a heating rate of 200 °C/min and a pressure of ~10 MPa were used; (iii) From 1100 °C to final temperature a heating rate of 50 °C/min and pressure of 100 MPa were used. The final temperature reached was 1150 °C and it was maintained for 5 min applying a pressure of 100 MPa. Sintering cycle was performed under vacuum conditions. For comparison purpose monolithic alumina was also prepared.

2.2.3. Hot pressing (HP)

Monolithic alumina obtained by hot press at 1500 °C during 1 h, starting from the same raw material α-alumina powder was also studied. Hot pressing was performed under Ar atmosphere and the pressure held was 25 MPa for a 50 mm diameter disk.

2.3. Characterization

2.3.1. Microstructural characterization

The microstructure of sintered specimens was studied on fracture surfaces by Scanning Electron Microscopy (FE-SEM, FEI Nova NANOSEM 230). Bulk densities of sintered compacts were determined by the Archimedes method in water.

2.3.2. Mechanical properties

2.3.2.1. Vickers hardness and toughness.
The Vickers hardness, H_V, of the samples was determined by microindentation (Buehler model Micromet 5103) on sample surfaces polished down to 1 micron, applying a 1.96 N load with an indentation time of 10 s. The magnitude of the Vickers hardness was determined according to,

$$H_V = 1.854 \frac{P}{d^2} \qquad (1)$$

where P is the applied load (in N) and d is the diagonal length (in m).

The fracture toughness was also determined by microindentation (diamond indenter Leco 100-A, St. Joseph, MI), but, for this specific property, the applied load was 98 N with an indentation time of 10 s. The fracture toughness was calculated using the formula given by Miranzo and Moya.[11]

2.3.2.2. Flexural strength.
The bending strength, σ_f, was determined by three-point bending test using prismatic bars cut from the pieces previously fired with 4 mm width, 30 mm length and 3 mm thickness. The tensile surfaces were polished down to 1 μm. The tests were performed at room temperature using a 5 kN universal testing machine SHIMADZU AutoGraph AG-X. The specimens were loaded to failure with a cross-head speed of 0.5 mm/min and a span of 20 mm.

2.3.2.3. Tribological behaviour.
The wear resistance of nanocomposites as well as alumina ceramic sintered by different techniques was studied under dry conditions. A "ball-on-disk" type wear test was performed under ambient dry conditions in a Microtest tribometer (model MT/60/NI) in conformity with ASTM G99, using alumina balls and being the disks the materials tested.

In this case, 3 mm diameter 99.9% pure alumina balls slid on the materials with a rotating speed of 3 rps and a radius of 0.8 mm. The applied load (F_N) was 10 N corresponding to initial Hertzian contact pressures of 2.5 GPa and tests lasted 60 h, which corresponded to a sliding distance (S) of ~3255 m. This load was carefully chosen in order to be located at the transition wear, in the vicinity of the severe wear region for the monolithic alumina, just to analyze the differences between the wear behaviour corresponding to the monolithic ceramic and the one of the nanocomposites. Before each test, the specimens and balls were rinsed ultrasonically in acetone. After each sliding test, the worn surfaces were cleared by blowing pressurized air before post-mortem observations. All tests were performed under the same conditions. Samples and alumina balls were weighed before and after the tests, but no significantly differ-
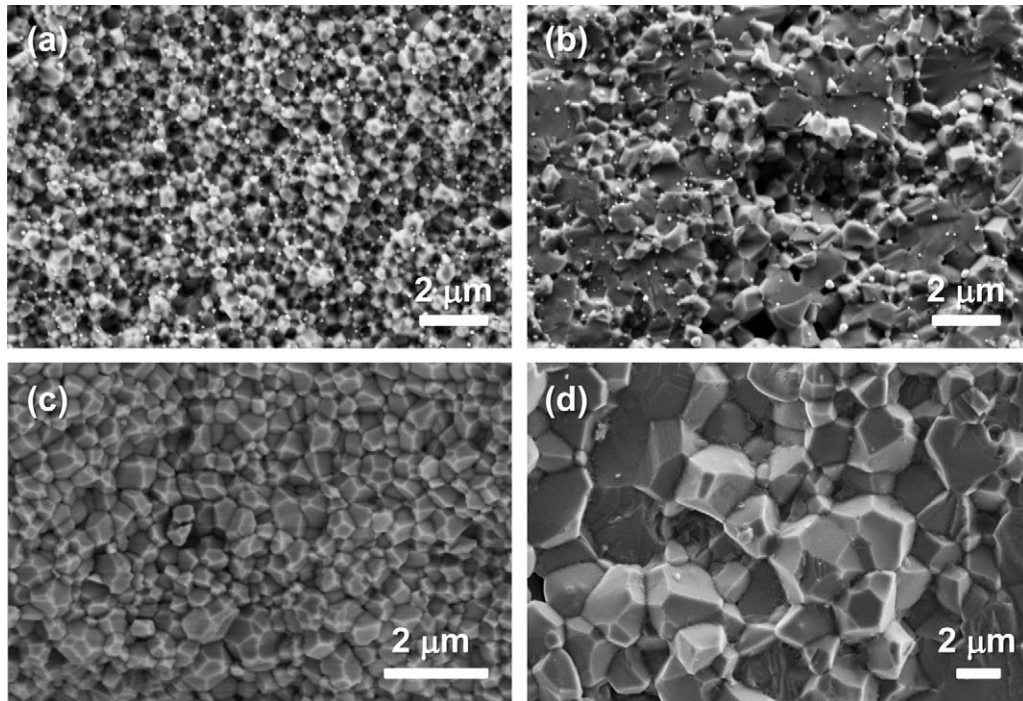
Fig. 1. Fracture surfaces SEM micrographs corresponding to (a) SPSed Al_2O_3/nNi, (b) CSed Al_2O_3/nNi, (c) SPSed Al_2O_3 and (d) HPed Al_2O_3.

ence in weights (Δm) were found. So the following wear rate equation was applied:

$$W = \frac{\Delta V}{F_N S} \tag{2}$$

Being ΔV the volume loss after the tests (mm^3), F_N the applied load (N) and S the sliding distance (m).

In order to estimate the volume losses correctly, the track profiles were analysed with a 3D surface profilometer (Taylor–Hobson Talysurf) which maps the surface morphology by putting a stylus in mechanical contact with the sample, being the step 0.01 μm and the scanning speed 0.1 mm/s. Profilometer was used to determine three dimensional surface topographic maps, so track volumes were estimated and, hence, Eq. (2) could be applied.

3. Results and discussion

3.1. Microstructural analysis

Fig. 1 shows SEM micrographs corresponding to fracture surfaces for SPSed and conventional sintered (CSed) Al_2O_3/Ni nanocomposites as well as SPSed and Hot Pressed (HPed) monolithic Al_2O_3. Ni nanoparticles and Al_2O_3 grains are the brighter and darker phases, respectively. As can be seen, Ni is

well dispersed in the alumina matrix independently of the sintering technique employed; this proves that the nanopowders were properly processed.

Differences in alumina and nickel mean grain sizes depending on the sintering technique used were observed, as shown in Table 1.

SPS is an adequate technique in order to constrain nanostructures as SPSed nanocomposites present the smallest alumina and nickel mean grain sizes. Microstructural refinement can be observed in composites (Fig. 1(a) and (b)) induced by the pinning effect held by Ni particles.

3.2. Mechanical properties and tribological behaviour

Several mechanical properties such as Vickers hardness (H_v), toughness (K_{IC}) and flexural strength (σ_f) together with wear resistance (W) were evaluated.

3.3. Vickers hardness, toughness and flexural strength

These experimental results are reported in Table 2, together with their Archimedes density measurements (all relative densities were found to be >98% th.).

Alumina/Ni nanocomposites present higher hardness values. The SPSed compact is the hardest one and this fact is related to

Table 1
Alumina matrix and Ni reinforcement mean grain sizes as a function of sintering technique used.

Material	Al_2O_3/nNi (SPS)	Al_2O_3/nNi (CS)	Al_2O_3 (SPS)	Al_2O_3 (HP)
Al_2O_3 grain size (μm)	0.25 ± 0.10	0.80 ± 0.20	0.40 ± 0.15	2.00 ± 0.50
Ni grain size (nm)	50 ± 18	110 ± 36	–	–

Table 2
Mechanical properties of materials sintered under different conditions.

Material	Al$_2$O$_3$/nNi (SPS)	Al$_2$O$_3$/nNi (CS)	Al$_2$O$_3$ (SPS)	Al$_2$O$_3$ (HP)
ρ (g/cm^3)	4.05 ± 0.01	4.05 ± 0.01	3.93 ± 0.01	3.97 ± 0.01
H_V (GPa)	25.0 ± 0.9	22.0 ± 0.3	21.8 ± 1.3	20.0 ± 0.2
K_{IC} (MPa m$^{1/2}$)	3.4 ± 0.2	4.8 ± 0.3	3.4 ± 0.2	3.8 ± 0.3
σ_f (MPa)	516 ± 28	626 ± 28	439 ± 70	520 ± 13

the smallest matrix grain size as well as the role that Ni nanoparticles play.[3] As alumina mean grain size increases, independently on the sintering technique, hardness value decreases. In the particular case of CSed alumina/Ni nanocomposite, the hardness value is also higher than values obtained for both monolithic aluminas (SPSed and HPed), but is not as high as the one corresponding to the SPSed alumina/Ni nanocomposite. Hardness improvement is related to the presence of Ni particles with sizes <50–60 nm.[3] When powders are conventionally sintered, Ni particles trend to grow, but still a fraction of them remains under this critical value, conferring CSed nanocomposites a hardness improvement, but not as significant as the one obtained by SPS. The latter technique preserves nanostructure, constraining the size of a very important fraction of Ni particles below this critical value.

The hardening magnitude is directly related to the distribution and size of Ni particles into the matrix and the hardening mechanism is the same for both composites, being Ni nanoparticles responsible of hardness improvement.[2,3] By SPS, nanostructures are preserved, alumina grains do not significantly grow (when comparing to raw material) and, due to the low sintering temperature, Ni nanoparticles remain under the critical size for inducing the hardening effect to the matrix. On the other hand, when conventional sintering is employed, higher temperatures are needed for composites consolidation. Alumina grains trend to grow but not in a dramatically way, due to the pinning effect held by Ni inclusions. By employing the conventional sintering technique, a fraction of Ni particles trend to grow giving sizes over the critical value which do not produce a hardening effect, but can assume plastic deformation and, hence, improve material toughness. But it remains another fraction of Nickel nanoparticles with sizes bellow the critical value and these nanoparticles are responsible of the hardness improvement achieved for the CSed nanocomposites.

Flexural strength corresponding to alumina/Ni nanocomposites has also been improved and this is a direct consequence of the microstructural refinement achieved by the inclusion of Ni nanoparticles (smaller flaw sizes). The values obtained for both nanocomposites are similar due to the balance between the higher toughness value of the CSed nanocomposites and their larger alumina matrix grain size.

Although (at these nanometric and submicrometric scale) there is not an obvious correlation between matrix grain size and K_{IC} values, this high toughness value obtained for CSed alumina/Ni nanocomposites is believed to be due to the presence of the intergranular plastic Ni particles (80–220 nm). Once the crack arrives at the Ni particle itself, the difference in the crack-tip opening displacement between the ductile particle and

the brittle matrix will cause the crack to be locally blunted and its segments forced to circumvent the particle, thus changing in propagation direction of the newly formed crack.[12–14] This mechanism can be justified by considering that over a certain critical size (≈50 nm for Ni), dislocations begin to be thermodynamically stable and plastic deformation can occur.[2] For CSed Al$_2$O$_3$/nNi composites, a not negligible number of Ni particles clearly present sizes over this critical value, so plastic deformation can take place and toughness can be improved with respect to SPSed nanocomposites. An important consequence of this mechanism is the change in fracture mode from
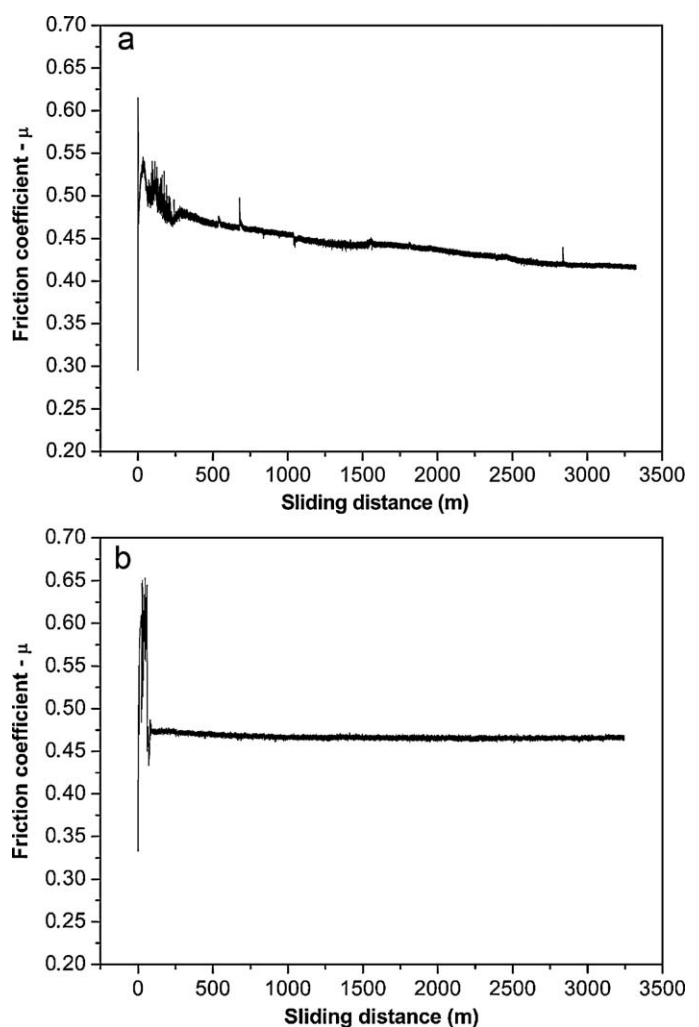

Fig. 2. Friction coefficient as function of sliding distance for (a) conventional and (b) spark plasma sintered Al$_2$O$_3$/nNi composites sliding at 0.02 m/s under a 10 N contact load against an alumina ball.

Table 3
Surface roughness (*Ra* and *Rt*) and friction coefficient (μ), for Al_2O_3/nNi composites (CS and SPS) and Al_2O_3 (SPS and HP) as function of sliding distance (*S*), when sliding at 0.02 m/s under 10 N load against alumina ball.

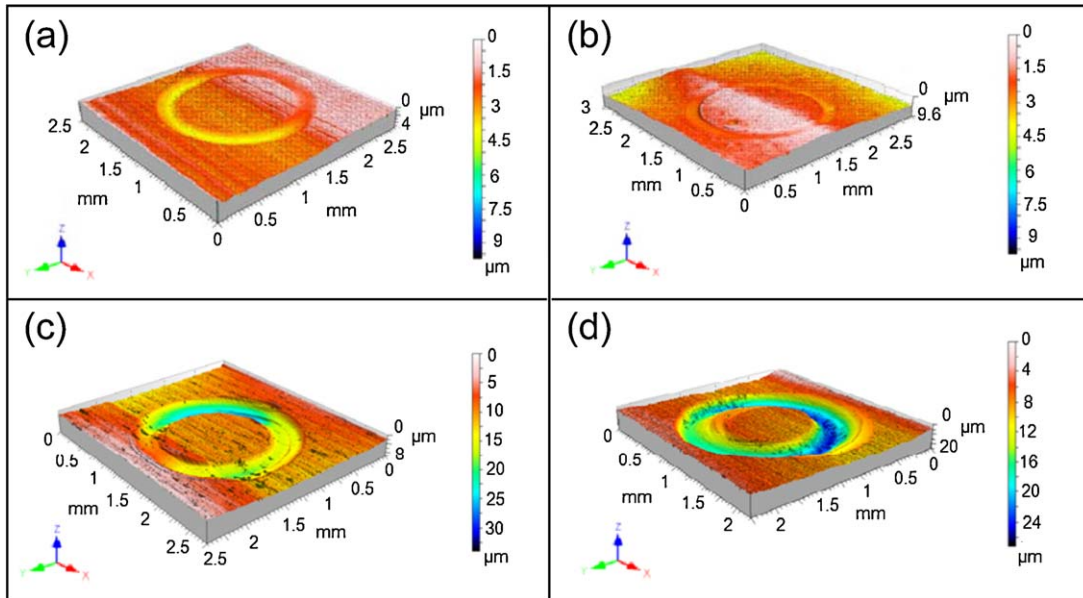|	*Ra* (μm)				*Rt* (μm)				μ
S (km)	0	0.10	1.50	3.25	0	0.10	1.50	3.25	–
Al_2O_3/nNi SPS	0.36	0.27	0.12	0.11	1.11	0.62	0.31	0.29	0.41
Al_2O_3/nNi CS	0.41	0.32	0.14	0.11	1.12	0.61	0.29	0.29	0.41
Al_2O_3 SPS	0.37	0.29	0.16	0.11	1.14	0.71	0.36	0.29	0.43
Al_2O_3 HP	0.51	0.43	0.30	0.14	1.42	1.02	0.39	0.35	0.43

Fig. 3. 3D final wear track topographies corresponding to (a) SPSed Al_2O_3/nNi, (b) CSed Al_2O_3/nNi, (c) SPSed Al_2O_3 and (d) HPed Al_2O_3 as a function of depth (coloured scale). In all cases $S = 3.25$ km, $F_N = 10$ N and $V = 0.02$ m/s.

intergranular fracture (for both monolithic alumina (SPS and HP) and for SPSed nanocomposite) to higher than 50% transgranular fracture for the CSed alumina/Ni nanocomposites (see Fig. 1). In the latter case, in which the alumina grain sizes are small (<2 μm) and equiaxed in nature, the fracture energy for cleavage (transgranular) fracture is higher than that for grain boundary (intergranular) fracture, that result in an improvement of fracture toughness. For the case of the monolithic alumina and SPSed nanocomposite, since the fracture resistance of the grain boundary is usually lower than that of the grain lattice, the crack will propagate intergranularly. Therefore, for CSed alumina/Ni nanocomposites, the intergranular Ni particles contribute to the reinforcement of the interface causing transgranular fracture.

3.4. Tribological behaviour

Different plots corresponding to the friction coefficients registered for a 10 N load of both Al_2O_3/nNi nanocomposite (CS and SPS) during the wear test are shown, as an example, in Fig. 2. All materials tested exhibit similar behaviour. The friction coefficient increases rapidly throughout the first meters of sliding and subsequently decreases. After this initial stage, the variations in the curves become smaller and the friction coefficient slightly increases during the remaining testing time.

This behaviour can be attributed to a polishing process during the wear test, establishing a smooth wear track surface, by ploughing away the surface asperities or roughness irregularities.

As long as the wear test advances, wear tracks become smoother and friction coefficients reach a steady state. This polishing mechanism is summarized in Table 3, in which the *Ra* and *Rt*, surface roughness before and after wear tests, are compared for all samples at different sliding distances. It is obvious that the roughness diminishes strongly during the first meters of sliding, and thus, the polishing effect is found to occur particularly within the running-in stage of the wear process.

Fig. 3 shows the surface topography of the three-dimensional wear tracks for all materials studied after sliding against pure alumina ball. From the 3D wear track surface topographies, the corresponding wear track dimensions, as well as the wear volume loss (*W*), were estimated and summarized in Table 4. All estimations made range from 10^{-6} to 10^{-8} (mm^3/N m), that means a difference of 2 orders of magnitude between the lowest and the highest rate calculated. The smallest wear track was measured for the CSed nanocomposite, while the highest wear values were obtained for the HPed alumina. The wear rate difference between the CSed and SPSed composite is 0.5 orders of magnitude. The difference in wear rate of alu-

Table 4

Track dimensions and wear values (W) obtained for Al_2O_3/nNi (SPS), Al_2O_3/nNi (CS), Al_2O_3 (SPS) and Al_2O_3 (HP) when slid against pure alumina ball ($S = 3.25$ km, $F_N = 10$ N, $V = 0.02$ m/s).

Material	Width (μm)	Depth (μm)	W (mm^3/N m)
Al_2O_3/nNi SPS	241	3.9	8.1×10^{-8}
Al_2O_3/nNi CS	196	2.5	2.6×10^{-8}
Al_2O_3 SPS	332	7.9	4.6×10^{-7}
Al_2O_3 HP	537	22.3	2.0×10^{-6}
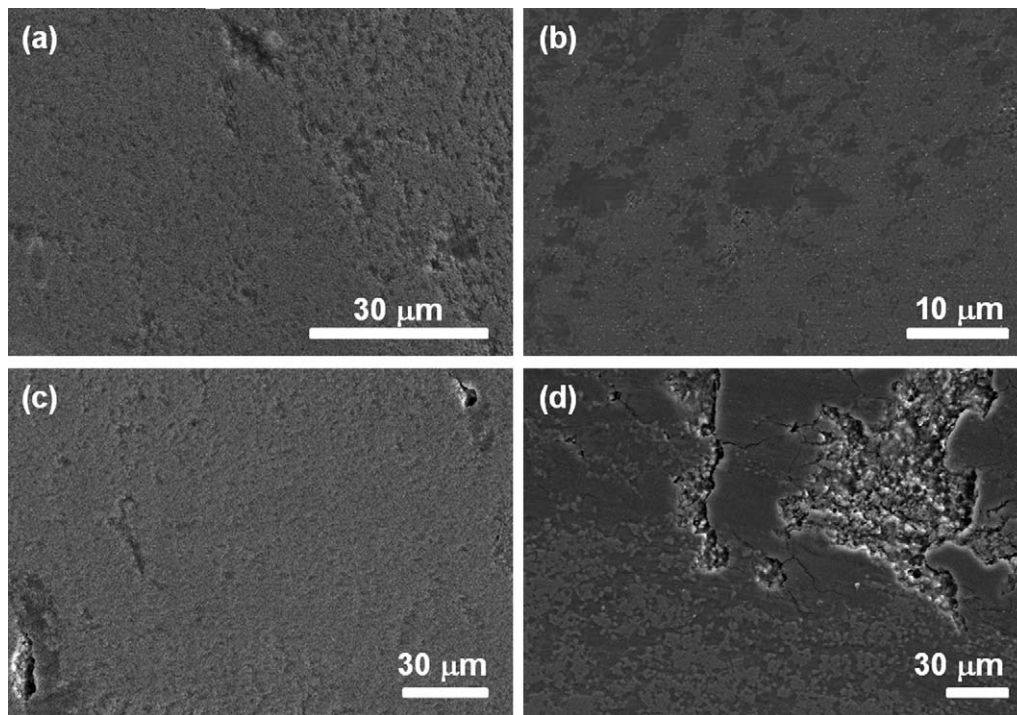
Fig. 4. Worn surfaces SEM micrographs of the (a) SPSed Al_2O_3/nNi, (b) CSed Al_2O_3/nNi, (c) SPSed Al_2O_3 and (d) HPed Al_2O_3.

mina sintered under different conditions is almost 1 order of magnitude, being smaller the value estimated for the SPSed alumina.

Further examinations of materials wear tracks confirmed the different wear rates observed that is related to fundamental changes in wear processes. Fig. 4(a–c) shows SEM micrographs corresponding to the worn surfaces of the SPSed and CSed nanocomposites and SPSed alumina, respectively, after tribotesting. For these three materials, a relatively smooth region can be observed while small particle size of the wear debris is an indicative that they were probably removed from the material by plastic deformation. In the SPSed materials cases, occasional evidence of pull out was observed. Inhibition of grain boundary cracking in the CSed nanocomposites will result in very limited material removal by the growth of intergranular cracks leading to grain pull-out.

In contrast, the hot pressed alumina worn surface generated under the same sliding conditions was generally rough (Fig. 4(d)). Noticeable evidence of pull-out was observed. This morphology is generated by an intergranular fracture mechanism where material removal is dominant.

It is well known that materials wear can be optimized by taking into consideration different facts: (i) microstructural refinement is beneficial for wear resistance since it retards transition to severe wear and hence, lower the mild or moderate wear rate; (ii) the harder the material, the lower will be the speed of introducing dislocations and so the stress accumulation at grain boundaries. In this sense, transition times towards severe wear will be higher; (iii) as toughness increases at grain boundaries, transition times to severe wear will also be increased and lowers the severe wear rate, (iv) if contact roughness decreases, for example by lubrication or polishing, moderate wear will be lower, as well the transition time to severe wear increases and also (v) minimizing residual stress as a consequence of sintering process (i.e. conventional sintering vs. SPS).

According to the second fact stated above, the best wear resistance should have been achieved for SPSed Al_2O_3/Ni nanocomposites, although they present lower fracture toughness and higher tendency to microcrack initiation and propagation.

The requirement of high hardness as a prerequisite for high wear resistance (abrasive) of hard ceramics has been questioned by Roberts.[15] In this work, it is described that

the depths of cracks produced by hard abrading particles in ceramic counterfaces were found to decrease with decreasing counterface hardness. For softer counterfaces, the load applied to the surface being abraded may fall below the minimum required to cause any indentation fracture, thus completely eliminating the loss of material by crack formation and grain pull-out.

Under the wear conditions essayed, it has been observed that not only hardness but also toughness are both parameters limiting the wear behaviour. When moving towards severe regime, toughness begins to play a crucial role. The synergy between relatively small matrix grains size together with the Ni particles acting as reinforcement, confers these CSed Al_2O_3/Ni nanocomposites remarkably good mechanical and tribological properties.

4. Conclusions

It is possible to fabricate by conventional sintering technologies Al_2O_3/nNi composites with very low wear rate combined with a high toughness value. The conventional sintered nanocomposite wear resistance at contact loads of 10 N was found to be higher than that of the SPSed nanocomposite, SPSed Alumina and hot pressed alumina by a factor of 0.5, 1 and 2 orders of magnitude, respectively.

These results clearly point out that the conventional sintered Al_2O_3/nNi composites can be considered as excellent candidates for wear resistant components as well as for cutting tools due to the superior cost per performance characteristics compare with other more complex processing routes like SPS or HP.

Acknowledgements

References

1. Moya JS, Lopez-Esteban S, Pecharromán C. The challenge of ceramic/metal microcomposites and nanocomposites. *Prog Mater Sci* 2007;**52**:1017–90.
2. Pecharromán C, Esteban-Betegón F, Bartolomé JF, Richter G, Moya JS. Theoretical model of hardening in zirconia–nickel nanoparticle composites. *Nano Lett* 2004;**4**:747–51.
3. Moya JS, Rodriguez-Suarez T, Lopez-Esteban S, Pecharromán C, Torrecillas R, Díaz LA, Nygren M. Diamond-like hardening of alumina/Ni nanocomposites. *Adv Eng Mater* 2007;**9**:898–901.
4. Rodriguez-Suarez T, Díaz LA, Torrecillas R, Lopez-Esteban S, Tuan W-H, Nygren M, Moya JS. Alumina/tungsten nanocomposites obtained by Spark Plasma Sintering. *Compos Sci Technol* 2009;**69**:2467–73.
5. Sekino T, Nakajima T, Ueda S, Niihara K. Reduction and sintering of a nickel-dispersed-alumina composite and its properties. *J Am Ceram Soc* 1997;**80**:1139–48.
6. Sekino T, Nakajima T, Niihara K. Mechanical and magnetic properties of nickel dispersed alumina-based nanocomposite. *Mater Lett* 1996;**29**:165–9.
7. Chen RZ, Tuan W-H. Pressureless sintering of Al_2O_3/Ni nanocomposites. *J Eur Ceram Soc* 1999;**19**:463–8.
8. Pecharromán C, Beltrán JI, Esteban-Betegón F, Lopez-Esteban S, Bartolomé JF, Muñoz MC, Moya JS. Zirconia/nickel interfaces in micro- and nanocomposites. *Z Metallkd* 2005;**96**:507–14.
9. Lopez-Esteban S, Gutierrez-Gonzalez CF, Mata-Osoro G, Pecharroman C, Diaz LA, Torrecillas R, Moya JS. Electrical discharge machining of ceramic/semiconductor/metal nanocomposites. *Scripta Mater* 2010;**63**:219–22.
10. Ortiz-Merino JL, Todd RI. Relationship between wear rate, surface pull-out and microstructure during abrasive wear of alumina and alumina/SiC nanocomposites. *Acta Mater* 2005;**53**:3345–57.
11. Miranzo P, Moya JS. Elastic/plastic indentation in ceramics: a fracture toughness determination method. *Ceram Int* 1984;**10**:147–52.
12. Bartolomé JF, De Aza AH, Martin A, Pastor JY, Llorca J, Torrecillas R, Bruno G. Alumina/zirconia micro/nanocomposites: a new material for biomedical applications with superior sliding wear resistance. *J Am Ceram Soc* 2007;**90**:3177–84.
13. Lieberthal M, Kaplan WD. Processing and properties of Al_2O_3 nanocomposites reinforced with sub-micron Ni and $NiAl_2O_4$. *Mat Sci Eng A* 2001;**302**:83–91.
14. Aharon O, Bar-Ziv S, Gorni D, Cohen-Hyams T, Kaplan WD. Residual stresses and magnetic properties of alumina–nickel nanocomposites. *Scripta Mater* 2004;**50**:1209–13.
15. Roberts SG. Depths of cracks produced by abrasion of brittle material. *Scripta Mater* 1998;**40**:101–8.